Optical and electrical properties of refined carbon derived from industrial tea waste

Materials Research Express

PAPER

Optical and electrical properties of refined carbon derived from industrial tea waste

Gökçen Akgül and Saliha Nur Bıçakçı

Recep Tayyip Erdogan University, Engineering Faculty, Department of Energy Systems Engineering, 53100, Rize, Turkey

E-mail: gokcen.akgul@erdogan.edu.tr

Keywords: tea waste, reduced graphene oxide, optical, electrical, refined carbon

OPEN ACCESS

RECEIVED
3 February 2020

REVISED
6 April 2020

ACCEPTED FOR PUBLICATION
15 April 2020

PUBLISHED
27 April 2020

Abstract

The utilization of nano- and well-ordered carbon materials such as graphene especially in carbon-based electrical devices and in energy storage areas is becoming important in terms of developing economical methods and reducing the dimensions of the electrical devices. These applied carbon materials are mostly originated from fossil sources which are diminishing. Hence, renewable carbon resources are gaining importance. Biomass is the single renewable carbon resource and can be refined to highly ordered carbon materials such as graphene by top to down methods. In this work, industrial tea waste biomass was converted to carbonized material by pyrolysis and refined by some further chemical treatments towards the ordered structured carbon. The newly derived refined carbon material was characterized by Raman, TGA, FTIR, SEM and XRD methods, and its optical and electrical properties were determined. The experimental results showed that the band gap energies of refined carbon derived from tea waste and reduced graphene oxide prepared in this study are in the similar level as 2.375 and 2.264 eV, respectively. Furthermore, the electrical conductivities are at the same stage as 3.16 and 3.28 $\times$ 10^{-4} $(1/\Omega{\cdot}cm)$ for reduced graphene oxide and refined carbon. The optically active and electrical conductive refined carbon material from biomass could be a proper carbon in energy related applications in terms of renewable and sustainable processing.

1. Introduction

Carbon as the main skeleton element of the world life, is a fascinating material that being found many industrial and scientific application areas such as; energy storage, health, catalysts and composite materials [1, 2]. Refined, high performance, well defined, porous or nano-scale carbon materials are required for the high technology applications i.e. biosensors and transistors [3, 4]. Carbon materials are desired to have properties of optical activity, thermal-chemical-mechanical stability and electrical conductivity observed in graphene, carbon nanotubes, nanoribbons etc [5].

The high performance carbon materials are mostly originated from fossil sources like coal, oil, turf or natural gas. These fossil sources are processed at high temperatures (2000 °C–3000 °C) and with high cost chemical-physical treatments such as chemical vapor deposition or gas phase synthesis for transferring them to well qualified materials. Since the fossil fuel sources are diminishing and the treatment processing costs, alternative and cheaper carbon sources are required.

Biomass, the only renewable carbon resource, can be used as alternative and sustainable reserve for the development of high performance carbon materials [6]. Pyrolysis is the first step to increase the carbon ratio, orientate the carbon structure and remove the volatile materials of the biomass [7]. This carbonized material which is mostly structured amorphously can be refined further by physical or chemical treatments to well-qualifed carbon. Generally, top to down methods are applied to amorphous carbon for obtaining well-ordered carbon like graphene that includes exfoliation, annealing, arc-discharge or oxygen reduction methods [6]. Yuan *et al* [8] reported the *in situ* formation of graphene from biomass tar by pyrolysis at 600 °C with the help of oxygen reduction method. Chen *et al* [9] synthesized high-quality graphene sheets from wheat straw via

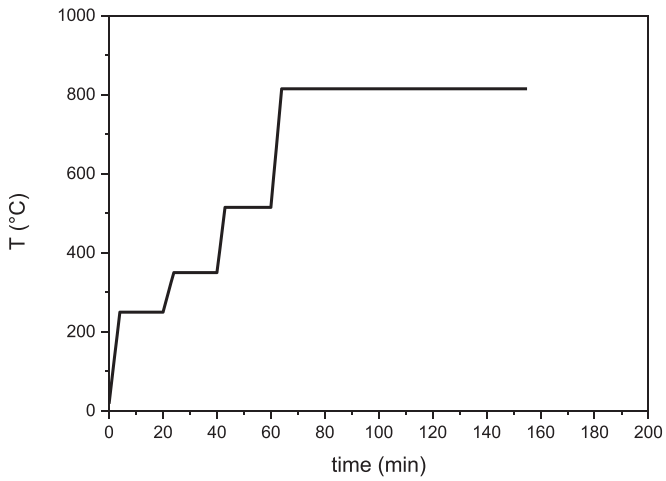

Figure 1. Heating program applied during pyrolysis.

graphitization by hydrothermal treatment and pyrolysis with the help of KOH catalyst. The derived high-quality graphene sheets employed as an excellent anode material for lithium ion batteries. Jurca *et al* [10] obtained graphene by pyrolysis of chitosan at 900 °C under argon atmosphere.

Various biomass resources can be considered as a proper candidate to obtain refined carbon; rice straw [11], corn stover [12], bamboo [13] or others [14]. In this work, industrial tea waste biomass was converted to carbon by pyrolysis, graphitization (oxygen reduction) and chemical treatment approaches. The optical and electrical properties of the derived refined carbon were determined that reveals if the carbon material could be a proper material in energy related applications.

2. Experimental

2.1. Derivation of refined carbon from tea waste

The tea waste obtained from a local tea industry in the form of straw (<2.36 mm) was grinded and sieved from 0.5 mm sieve. The raw tea waste sample was dried overnight at 80 °C and then impregnated with saturated $FeCl_3$ (Tekkim) solution with the ratio of 3:1 (w/w) as tea waste : $FeCl_3$. Re-dried sample was pyrolysed in a rotary oven (Protherm RTR 11/100/500) at the 815 °C at N_2 atmosphere (1 l min^{-1}) for 1.5 h. The heating program is given in figure 1. The sample was let to cool down itself under continuing N_2 flow to room temperature. The total pyrolysis time is around 3.5 h.

The carbonized sample was pulverised (Frithsch Pulverisette 9) at 850 rpm for 10 min and sieved from 25 μm. The <25 μm carbon sample was washed with concentrated acids (6M HCl, then 6M HF) to remove the impregnated iron and the other possible minerals biomass included. Thereafter, sample neutralized by washing with de-ionised water was dried again. The sample was nomenclatured as BC-Fe-Y.

BC-Fe-Y was further treated by modified Hummers method to refine the structure towards the graphene oxide-like one (BC-Fe-Y-R). The reduction of the oxides was performed with a reduction agent of hydrazine (Merck). The obtained carbon was named as BC-Fe-Y-rR. As a comparison material, reduced graphene oxide was derived from a commercial graphite (SBM teknik) as well [15–17].

2.2. Characterizations of carbon samples

The structure of the carbon samples was characterized by Raman (Micro RamanWitec Alpha 300R, 532 nm), FTIR (Perkin Elmer Spectrum 100), XRD (Rigaku SmartLab X-ray diffractometer non-monochromatographic Cu Kα1-radiation (40 kV, 30 mA, $\lambda = 1.54$ A°)), SEM (Jeol JSM-6610) and TGA (Schimadzu TGA50 Analyser, 20 °C min^{-1}, air atmosphere).

The optical measurements were performed to determine the band gaps of the samples. The principle is based on the absorption of the monochromatic light at UV and/or visible wavelength by the sample. The carbon samples were mixed in N-Methyl-2-pyrrolidone (NMP) that ordered carbon (graphene-like) is penetrate into the solution (figure 2(a)) which was then centrifuged and the supernatant was placed on a cleaned glass wafer (1 × 1.5 cm). Around 150 nm thin film emerged on the glass surface by several times dripping the solution and simultaneous drying on a hot plate at around 80 °C (figure 2(b)). The prepared wafers were scanned with the light beam with the wavelength from 350 to 1000 nm (Spectra Max M5 Analyser). The absorbance coefficient

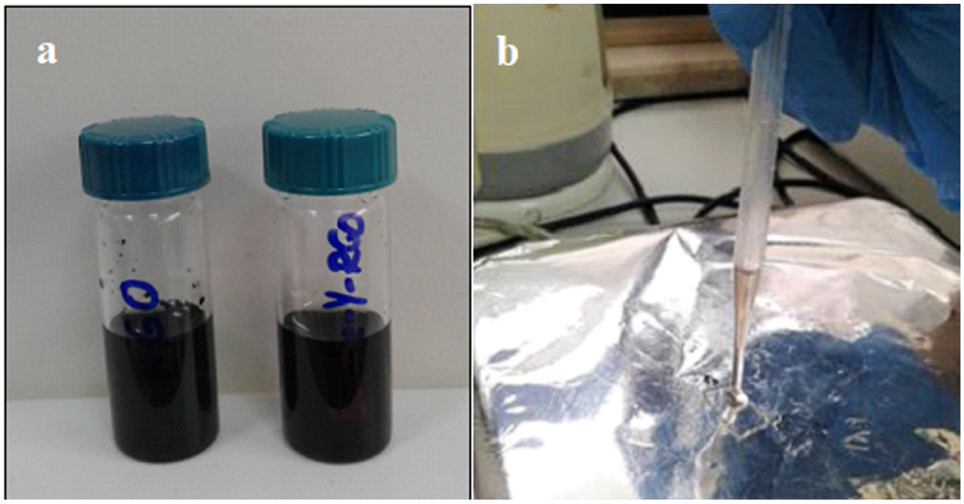

Figure 2. (a) the NMP solutions of the rGO and BC-Fe-Y-rR, (b) placing the carbon solution on a glass wafer.

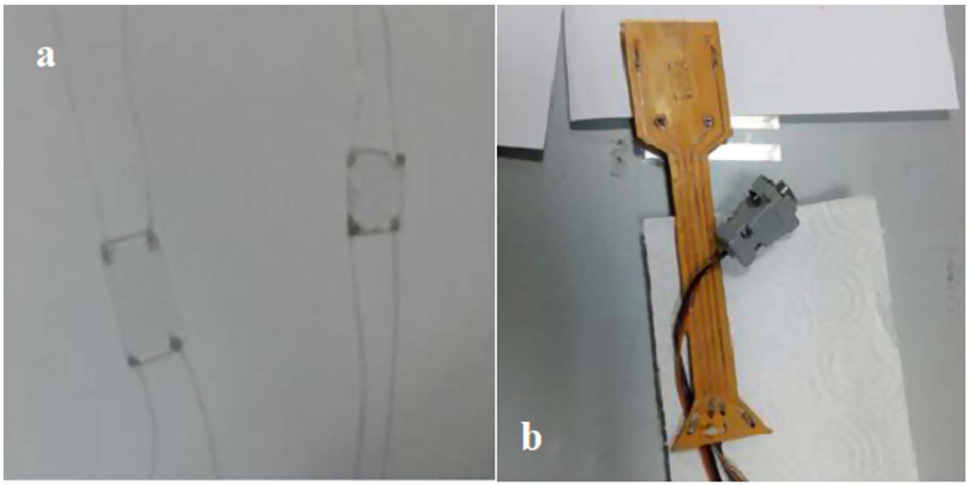

Figure 3. (a) four point contacted glass wafers, (b) electrical measurement sample setup.

was calculated according to equation (1).

$$\propto = -\ln\left(\frac{1}{T}\right) \cdot \left(\frac{1}{d}\right) \tag{1}$$

where $\propto$ is the absorbance coefficient, d is the thickness of the film and T is the transmittance value at the set wavelength. The forbidden bandgap energy E_g was determined from the graph of $\propto \cdot (h \cdot \vartheta)^2$ versus $h \cdot \vartheta$, where h is the Planck constant, ϑ is the frequency (c/λ, c is the velocity of light, λ is the wavelength of the scanning light).

The electrical measurements were performed by Van der Pauw four point and Hall effect methods with the aid of Keithely 2410 source meter in the four-probes configuration. The four point ohmic contacts were settled on the thin filmed glass wafer surface with the indium solder (figure 3(a)). The resistivity and the charge density were determined by the principle of switching on the current (I) at the first and fourth points and measuring the potential (V) from the second and the third points (figure 3(b)). I_{14}, I_{43}, I_{32}, I_{21} currents were applied and V_{23}, V_{12}, V_{41}, V_{34} were determined. Same current layout was performed that I_{41}, I_{34}, I_{23}, I_{12} currents were applied and V_{32}, V_{21}, V_{14}, V_{43} potentials were determined. According to Ohm law, the resistivity is given as in equation (2).

$$R_{21,34} = \frac{V_{34}}{I_{21}} \tag{2}$$

Similar to equation (1), $R_{32,41}$, $R_{23,14}$, $R_{43,12}$, $R_{21,34}$, $R_{14,23}$, $R_{41,32}$ were obtained. The specific resistivity (ρ) is defined as in equation (3).

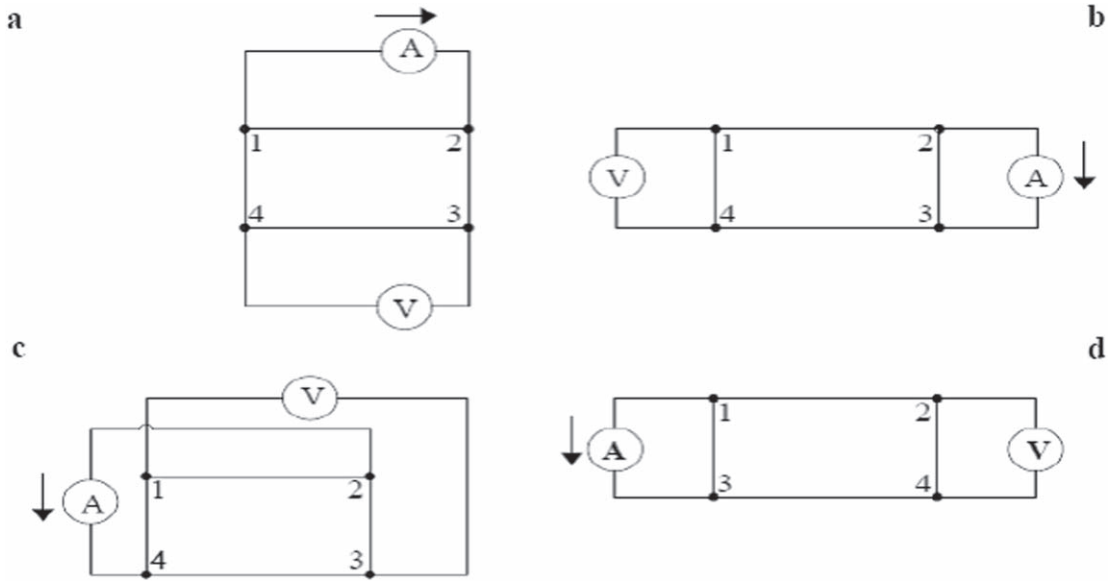

Figure 4. (a), (b) The Van der Pauw four-point resistivity measurement points, (c), (d) Hall effect carrier density measurement points.

$$\rho = \frac{\pi \cdot d}{\ln 2} \cdot \left(\frac{R_A + R_B}{2}\right) \cdot f\left(\frac{R_A}{R_B}\right) \tag{3}$$

where $f\left(\frac{R_A}{R_B}\right)$ is the correction factor. R_A and R_B are identified as in equations (4) and (5), respectively.

$$R_A = \frac{R_{21,34} + R_{12,43} + R_{43,12} + R_{34,21}}{4} \tag{4}$$

$$R_B = \frac{R_{32,41} + R_{23,14} + R_{14,23} + R_{41,23}}{4} \tag{5}$$

The specific conductivity (σ) is given as in equation (6).

$$\sigma = \frac{1}{\rho} \tag{6}$$

Figure 4 shows the current and potential points of the samples applied and determined, respectively. Measurements were performed in the dark chamber.

The charge density (n) of the thin film sample was determined by Hall effect measurements. The current (I) was applied to the sample thin film, four point contacted glass wafer was settled in a magnetic field perpendicular to the surface and the resistivity (R_H) was measured. The Hall potential (V_H) is determined by equation (7).

$$V_H = R_H \cdot \frac{I \cdot \vec{B}}{b} \tag{7}$$

where b is the size of the sample, $\vec{B}$ is the magnetic field magnificent. When the currents of I_{13}, I_{31}, I_{24}, I_{42} were applied, V_{24}, V_{42}, V_{13}, V_{31} potentials were determined for electrons (N) and electron gaps (P), respectively. Herewith, V_H is defined as the total of V_C, V_D, V_E and V_F (equations (8)–(11)).

$$V_C = V_{24P} - V_{24N} \tag{8}$$

$$V_D = V_{42P} - V_{42N} \tag{9}$$

$$V_E = V_{13P} - V_{13N} \tag{10}$$

$$V_F = V_{31P} - V_{31N} \tag{11}$$

The charge density is calculated by equation (12).

$$n = 8 \cdot 10^{-8} \cdot \frac{I \cdot \vec{B}}{q.\, V_H \cdot d} \tag{12}$$

Where q is the electron charge.

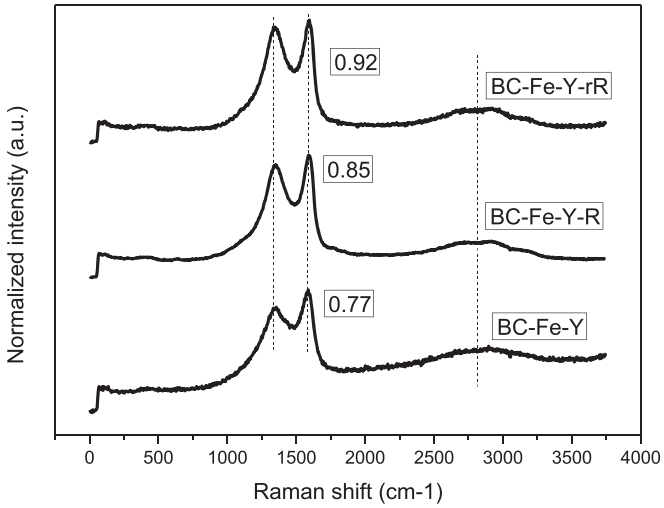

Figure 5. Raman analyses of the refined carbon samples.

3. Results and discussion

3.1. Structural characterizations of the carbon materials

The development of the structure of the carbon derived from tea waste was assessed by Raman Spectroscopy shown in figure 5. The band at 1350 cm^{-1} is the D-band while the 1590 cm^{-1} is the G-one which are the most basic features in determining the characteristic of defects and sp2 carbon features. Raman analyses for GO and rGO can be found in elsewhere [18]. Modified Hummers method for the synthesis of GO from graphite increases the ID/IG ratio from 0.09 to ~1.0 [19] and a greater number of defects form in GO which are used to obtain rGO. It presents the decrease in the crystal structure and the amorphization due to the oxygen functional groups and conversion of sp^2 to sp^3 bonds. The respective ID/IG ratios of GO and rGO are reported as 1.0 and 0.84 [19] that indicates the residual defects still stay in rGO. The ID/IG ratios of the samples in this work are 0.77 and 0.92 for BC-Fe-Y and BC-Fe-Y-rR, respectively. The BC-Fe-Y-R has an intermediate ID/IG ratio of 0.85. Oxidation of BC-Fe-Y has increased the D peak intensity and hence the ID/IG ratios. The oxy-groups of BC-Fe-Y-R could partly reduce but BC-Fe-Y-rR has still the highest ID/IG ratio. The FTIR results (figure 7) show that C=O strengths disappear when BC-Fe-Y-R reduces to BC-Fe-Y-rR which could cause C–O strengths and high ID/IG ratio for BC-Fe-Y-rR.

The broad 2D peak at ~2850 cm^{-1} is always present in graphenic structures since the oxygenated functional groups on the layers have resilience by steric effects and partial amorphization. Any defects are required for its activation [20].

Thermograms of the BC samples under air atmosphere are given in figures 6(a) and (b). TGA analyses indicate that successful mineral removal to negligible amounts (less than 5%wt.) was achieved for the samples. As further, treating the BC-Fe-Y by modified Hummers method oxygenates the starting carbon sample more which can cause less thermal stability of BC-Fe-Y-R than BC-Fe-Y-rR. Similar termogravimetric behavious were obtained for GO and rGO obtained from commercial graphite.

In FTIR spectra is given in figure 7 and the major peaks are listed in table 1.

The intense band between ~3670 and 2100 cm^{-1} with maxima at ~3100 cm^{-1} of GO is attributed to the –OH peak. The absorption band intensity corresponding to this oxygen functional groups decreases for rGO after reducing of GO. On the other hand, BC-Fe-Y-R and BC-Fe-Y-rR have a fairly broader peak from 3650 cm^{-1} to ~1800 cm^{-1} could include some peaks such as at ~2900 cm^{-1} for C–H stretching vibrations (a small shoulder is seen for GO) and at ~2100 cm^{-1} attributing C≡C bonds alongside of –OH strengths [21]. The oxygen containing functional groups would be responsible for the absorption peak around 2340 cm^{-1} seen for GO and rGO [19]. The peaks at ~2100–2000 cm^{-1} could be seen for graphite samples [22]. The fairly broad band of BC samples could show that the BC samples have more oxygenated functional groups on the surface than graphitic ones. Stretches of C=C at ~1580 cm^{-1} of GO and BC samples would be the result of unoxidized domain. The respective C=O and C–O strengths at ~1724 and ~1040 cm^{-1} are observed for GO due to possible COOH groups on the surface [23] while C=O peak disappears for BC-Fe-Y-rR. C–O–C strength is more efficient for BC samples. It seems that reduction eliminates some of the CO stretchings at GO more effective than biomass originated carbon samples.

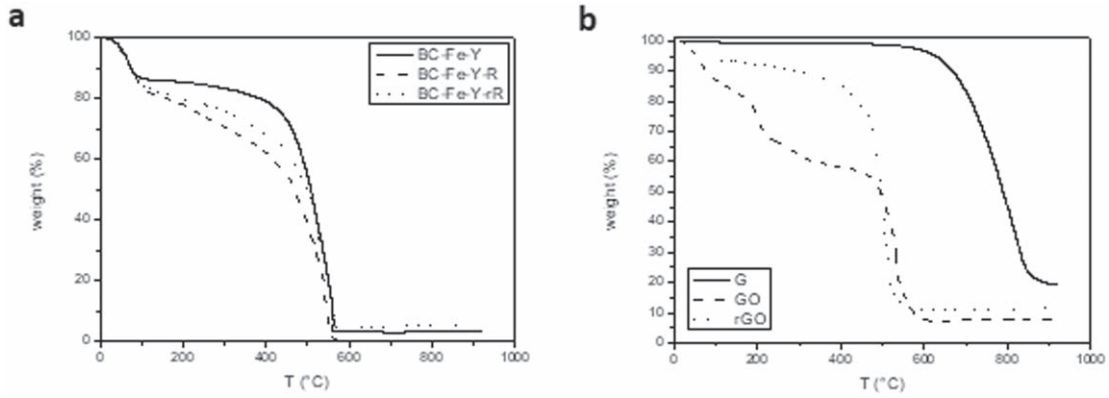

Figure 6. TGA analyses of the refined carbon samples (a) and graphitic carbon samples (b).

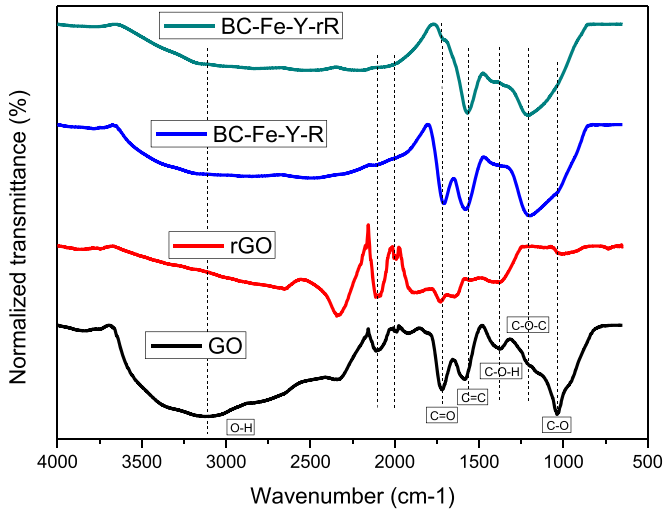

Figure 7. FTIR analyses of the samples.

Table 1. The major FTIR peaks of the samples.

Wavenumber (cm^{-1})	Vibrational assignments
3673–2640	O–H
1724	C=O
1580	C=C
1380	C–OH
1205	C–O–C
1040	C–O

The characteristic XRD diffraction patterns of the samples (figure 8) are examined as stark peak at ~24° and 10° and a weak peak around 42°. The peaks at 10° and 42° are typical peaks for GO by their Miller indices of 002 and 100, respectively. The broad peak appears at around 24° (002) corresponds the amorphous carbon structure that the increasing intensity shows the structural ordering from BC-Fe-Y-R to rGO by reduction.

The morphology of the samples was investigated through SEM analyses (×2000, 15 kV). Figure 9 represents crumbled structure for BC samples whereas crumpled, rippled and layered structures are seen for GO and rGO.

3.2. Optical and electrical characterizations

The optical transparencies of BC-Fe-Y-rR and rGO are shown in figure 10. The absorbance coefficient $\propto$ was calculated from the transparency according to equation (1). and the bandgap energy E_g was determined as

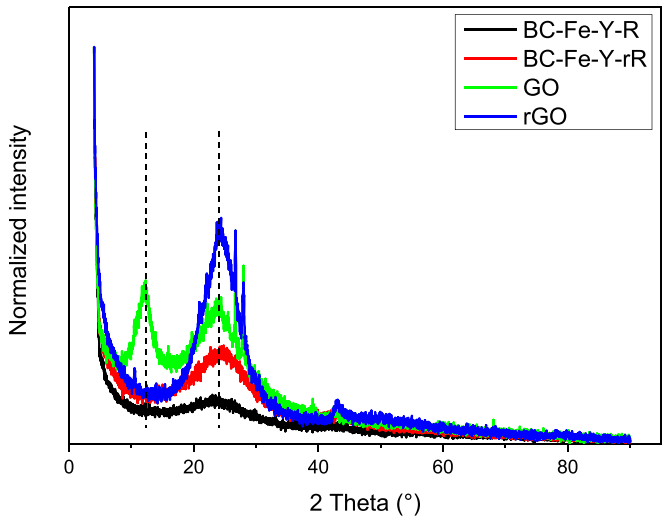

Figure 8. XRD analyses of the samples.

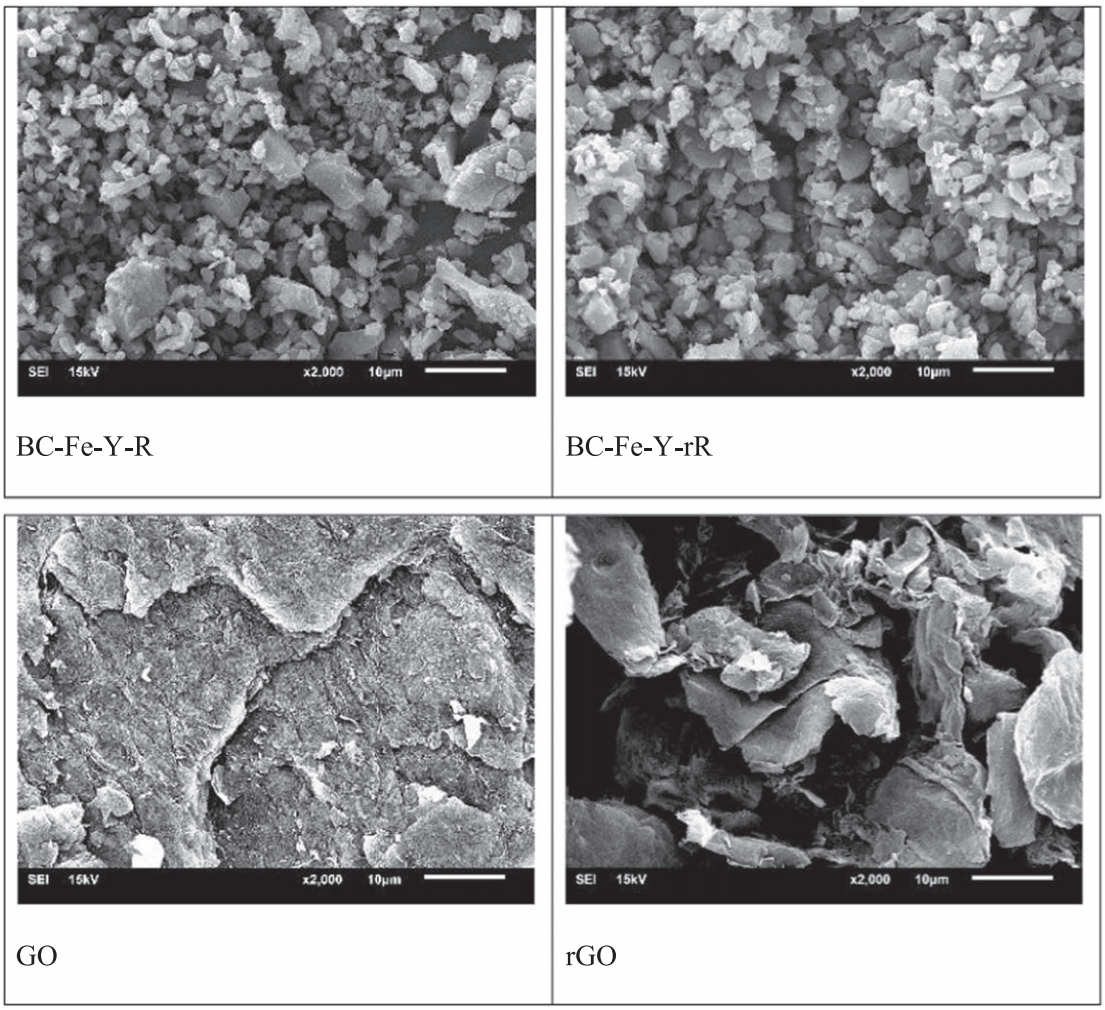

Figure 9. SEM pictures of the samples.

2.264 eV and 2.375 eV for rGO and BC-Fe-Y-rR, respectively (figure 11). Approximate E_g values for BC-Fe-Y-rR and rGO samples show the amorphous carbon structure was developed towards the ordered one.

Mohandoss and Nelleri [24] determined the forbidden bandgap energy of natural sunlight reduced graphene oxide as 2.2 eV which is compatible with our results. While the single layer graphene is nearly transparent and

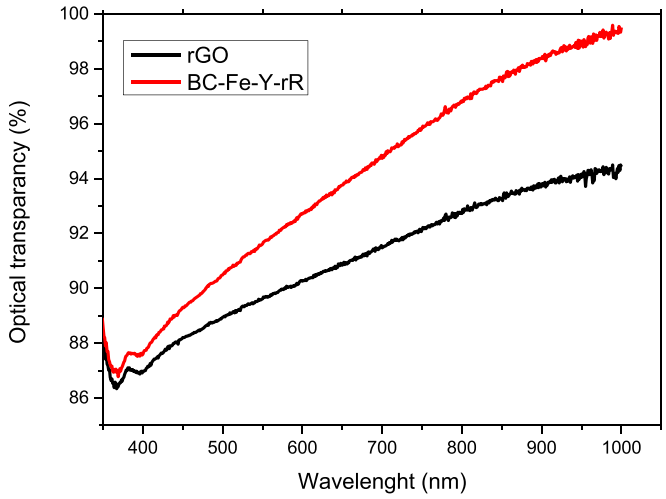

Figure 10. Optical scanning of the samples.

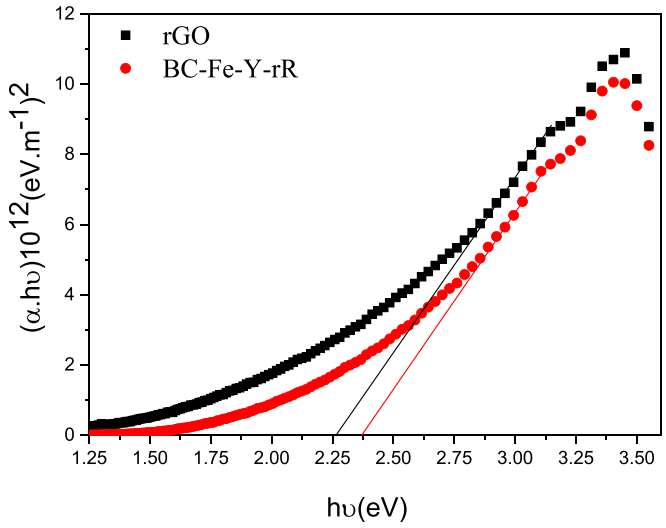

Figure 11. Indication of forbidden band gaps of the reduced graphene oxide samples.

Table 2. The electrical conductivity and charge densities of the carbon samples.

Sample	σ $(1/\Omega\cdot cm)\cdot 10^{-4}$	n $(cm^{-3})\cdot 10^{14}$
rGO	3.16	6.76
BC-Fe-Y-rR	3.28	1.00

has a zero band gap, every layers result the dropping of transmittance and electrical conductivity that offer usable applications of semiconductives in transistors, photovoltaic cells and electronics [25].

The specific conductivity σ and the charge density (n) were given in table 2. The electrical conductivities of the samples are in the same level. Although the charge density (n) of the BC-Fe-Y-rR is smaller than rGO, it is still in the same magnitude showing that the material is conductive.

Gabhi *et al* [26] reported the increasing of electrical conductivity of biochar obtained from various biomass such as sugar maple, oak, hickory, grass and bamboo by crystallization at higher pyrolysis temperatures in direction to graphene planes. When the carbonization of sugar maple increase from 87% to 95%, the electrical conductivity increased from 2.47×10^{-6} to 0.67 S cm^{-1} which are due to containing randomly oriented graphite/graphene sheets analytically supported. Sun *et al* [27] derived pyrogenic carbon by pyrolysis of black walnut at temperatures of 400°C–800°C and showed that electron transfer becomes faster since the carbon

structure is more ordered at higher temperatures. Furthermore, the surface functional groups contribute to the overall electron flux due to lower charging and discharging capacities.

Deng *et al* [7] reviewed the green synthesis of carbon nanomaterials of which electrical conductivity can be orders of magnitudes higher than copper and their high optical transmittance provides applications in communication devices. Transforming the waste biomass into optical active and electrical conductive carbon like graphene is gaining attention for energy related applications.

4. Conclusion

Large amount of industrial tea waste is emerging as a consequence of huge production of tea in the world. It is shown in this study that this biomass as a soft carbon resource can be refined to optically active and electrical conductive carbon material in terms of sustainable and renewable processing. Although BC samples are rich in stark surface functional groups than graphitic ones, exfoliating by Hummers method is still answers the purpose. The optically active and electrical conductive refined carbon material from tea waste could be a proper candidate material in carbon-based electrical devices.

Acknowledgments

We gratefully acknowledge the financial support provided by Recep Tayyip Erdogan University, Scientific Research Projects Coordinator Unit (BAP) (Project No: FYL-2018-970).

ORCID iDs

Gökçen Akgül https://orcid.org/0000-0001-6101-7971

References

[1] Thrower P A 2002 *Mol. Cryst. Liq. Cryst.* **386** 1
[2] Cab C, Canto G, Medina J and Tapia A 2018 *J. Nanomaterials* **2058613** 1
[3] Notarianni M, Liu J, Vernon K and Motta N 2016 *Beilstein J. Nanotechnol.* **7** 149
[4] Kamran U, Heo Y J, Lee J W and Park S J 2019 *Micromachines* **10** 1
[5] Candini A, Martini L, Chen Z, Mishra N, Convertino D, Coletti C, Narita A, Feng X, Müllen K and Affronte M 2017 *J. Phys. Chem.* C **121** 10620
[6] Lee X J, Hiew B Y Z, Lai K C, Lee L Y, Gan S, Thangalazhy-Gopakumar S and Rigby S 2019 *J. Taiwan Inst. Chem. Eng.* **98** 163
[7] Deng J, You Y, Sahajwalla V and Joshi R K 2016 *Carbon* **96** 105
[8] Yuan H, Chen H, Li D, Deng L, Chen J, Fan Y, He M and Sun F 2019 *Electrochem. Commun.* **100** 52
[9] Chen F, Yang J, Bai T, Long B and Zhou X 2016 *J. Electroanal. Chem.* **768** 18
[10] Jurca B, Bucur C, Primo A, Concepción P, Parvulescu V I and García H 2019 *Chem. Cat. Chem.* **11** 985
[11] Goswami S, Banerjee P, Datta S, Mukhopadhayay A and Das P 2017 *Process Saf. Environ. Prot.* **106** 163
[12] Jin H, Wang X, Shen Y and Gu Z 2014 *J. Anal. Appl. Pyrolysis* **110** 18
[13] Li S, Li X, Chen C, Wang H, Deng Q, Gong M and Li D 2016 *Compos. Sci. Technol.* **132** 31
[14] Wang J, Nie P, Ding B, Dong S, Hao X, Dou H and Zhang X 2017 *J. Mater. Chem.* A **5** 2411
[15] Pei S and Cheng H M 2012 *Carbon* **50** 3210
[16] Roy S 2017 *Am. J. Chem. Res.* **1** 0001
[17] Park S and Ruoff R S 2009 *Nat. Nanotechnol.* **4** 217
[18] Fu C, Zhao G, Zhang H and Li S 2013 *Int. J. Electrochem. Sci.* **8** 6269 ISSN 1452-3981
[19] Ossonon B D and B´elanger D 2017 *RSC Adv.* **7** 27224
[20] Ferrari A C and Basko D M 2013 *Nature Nanotech.* **8** 235
[21] Nanda S, Mohanty P, Pant K K, Naik S, Kozinski J A and Dalai A K 2013 *Bioenerg. Res.* **6** 663
[22] Ruiz S, Tamayo J A, Ospina J D, Porras D P N, Zapata M E V, Hernandez J H M, Valencia C H, Zuluaga F and Tovar C D G 2019 *Biomolec.* **9** 109
[23] Baibarac M, Baltog I and Szunerits S 2016 Raman and FTIR Spectroscopy as Valuable Tools for the Characterization of Graphene-Based Materials *Graphene Science Handbook* (Boca Raton, FL: CRC Press) 16
[24] Mohandoss M and Nelleri A 2018 *Opt. Mater.* **86** 126
[25] Baliga B J 2019 Introduction *Fundamentals of Power Semiconductor Devices* 2nd edn (Berlin: Springer) 1 1978-3-319-93987-2
[26] Gabhi R S, Kirk D W and Jia C Q 2017 *Carbon* **116** 435
[27] Sun T, Levin B D A, Guzman J J L, Enders A, Muller D A, Angenent L T and Lehmann J 2017 *Nat. Commun.* **8** 1